Journal of
Marine Science and Engineering

MDPI

Article

Elemental Composition of Particulate Matter in the Euphotic and Benthic Boundary Layers of the Barents and Norwegian Seas

Dina P. Starodymova *, Marina D. Kravchishina *, Anastasia I. Kochenkova, Alexey S. Lokhov, Natalia M. Makhnovich and Svetlana V. Vazyulya

Shirshov Institute of Oceanology, Russian Academy of Sciences, 36 Nakhimovsky Prosp., Moscow 117997, Russia
* Correspondence: d.smokie@gmail.com (D.P.S.); kravchishina@ocean.ru (M.D.K.)

Abstract: The increasing influence of Atlantic inflows in the Arctic Ocean in recent decades has had a potential impact on regional biogeochemical cycles of major and trace elements. The warm and salty Atlantic water, entering the Eurasian Basin through the Norwegian Sea margin and the Barents Sea, affects particle transport, sink, phyto-, and zooplankton community structure and could have far-reaching consequences for the marine ecosystems. This study discusses the elemental composition of suspended particulate matter and fluffy-layer suspended matter derived from samples collected in the Barents Sea and northern Norwegian Sea in August 2017. The mosaic distribution of SPM elemental composition is mainly determined by two factors: (i) The essential spatial variability of biological processes (primary production, abundance, and phytoplankton composition) and (ii) differences in the input of terrigenous sedimentary matter to the sea area from drainage sources (weak river runoff, melting of archipelago glaciers, etc.). The distribution of lithogenic, bioessential, and redox-sensitive groups of elements in the particulate matter was studied at full-depth profiles. Marine cycling of strontium in the Barents Sea is shown to be significantly affected by increasing coccolithophorid bloom, which is associated with Atlantic water. Mn, Cu, Cd, and Ba significantly enrich the suspended particulate matter of the benthic nepheloid layer relative to the fluffy layer particulate matter within the benthic boundary layer.

Keywords: suspended particulate matter; trace elements; major elements; euphotic layer; fluffy layer; particulate form; bioessential elements; the Barents Sea; the Norwegian Sea

check for updates

Citation: Starodymova, D.P.; Kravchishina, M.D.; Kochenkova, A.I.; Lokhov, A.S.; Makhnovich, N.M.; Vazyulya, S.V. Elemental Composition of Particulate Matter in the Euphotic and Benthic Boundary Layers of the Barents and Norwegian Seas. *J. Mar. Sci. Eng.* **2023**, *11*, 65. https://doi.org/10.3390/jmse11010065

Academic Editor: Antonio Cobelo-Garcia

Received: 19 November 2022
Revised: 19 December 2022
Accepted: 24 December 2022
Published: 2 January 2023

1. Introduction

The main features of suspended particulate matter (SPM) in marine waters are formed as a result of the mixing of mineral and biogenic particles. The mineral particle supply is mostly external, usually through atmospheric dust deposition, river input, and sedimentary resuspension, or is generated internally through the authigenic precipitation of minerals. The biogenic particles originate from the vital activity of marine organisms, namely the biological production of particulate organic matter (POM) and biominerals such as calcium carbonate ($CaCO_3$) and opal (biogenic silica, $BSiO_2$) [1,2]. Particle concentration is thought to be a major factor in controlling the scavenging of particle-reactive trace elements (TE) [3]. The SPM is concentrated in two layers of the water column, namely, the euphotic zone and the benthic boundary layer (BBL). Suspended particles of the euphotic zone are subjected to strong seasonal dynamics in high-latitude seas. The BBL is the layer of flowing seawater directly above the sediment at the benthic substrate. Important processes occur in the BBL that precede the formation of sediment, such as resuspension, lateral particle transport, particle aggregation [4], and biologically mediated particle deposition [5]. These processes largely determine the composition of the sediments. The lower, most particle-saturated part of the BBL is distinguished as the benthic nepheloid layer (BNL) [5]. It is therefore critical that we study the concentration and elemental composition of SPM in the euphotic

zone and the BBL of the water column and the fluffy layer suspended matter (FLSM) at the water–sediment interface. FLSM is a thin layer of fairly concentrated suspended matter resting on the sea floor [6] and enriched by a newly formed biomass of bacteria and archaea [7,8].

The present climate change in the Arctic has led to a dramatic shift in the ocean and atmosphere [9]. Volume exchange between the Arctic and the high latitude North Atlantic Oceans (>65° N) is controlled mostly by the Barents Sea Opening, located between Svalbard and coastal Norway and the Fram Strait, separating the Nordic Seas south of the Arctic Ocean [10]. The Barents Sea shelf became close to ice-free in the 2010s [11]. The long-term biogeochemical consequences of such changes remain unclear.

The elemental composition of SPM reflects the processes that occur with this material in the process of sedimentogenesis [1,2,12]. The composition of marine SPM depends on a number of closely related biological and physicochemical processes occurring in the water column (e.g., microalgae blooms, degradation of organic matter, redox reactions), as well as on hydrological conditions. The study of some elements in SPM is of great concern for establishing the patterns of sediment formation, which can be useful for paleooceanological reconstructions [13]. The distribution of SPM is governed by the principles of the circum-continental and climatic zones [1]. Tectonic zoning is also important for the Norwegian Sea since it is bordered by the Arctic Mid-Ocean Ridge (Mohns Ridge) in the west, where active submarine volcanoes and hydrothermal vents have been identified [14,15]. Hydrothermal plumes are a source of SPM, which contains ore minerals (such as barite and iron, copper, zinc sulfides, etc.) [16].

Studies of the SPM composition in the European Arctic seas were most active in the 1990s [17–23]. The distribution of the major particulate phases (particulate-forming constituents) in SPM, such as organic and carbonate matter, amorphous silica, lithogenic matter, Fe oxyhydroxides, Mn oxides, etc., is studied in more detail [24,25]. There are a few studies on the TE composition of SPM in this region, particularly in the Pechora Sea—SE part of the Barents Sea [26,27]; the Barents Sea proper [28]; the northern Barents Sea [29,30]; the Franz Victoria Trough [31]; in the Bear-Island Trough [32,33]; and at the K-278 Komsomolets soviet nuclear submarine crash site [20,21]. The TE composition of SPM in the BBL of the Barents Sea was reported [34]. It should be noted that previous studies were relatively local and did not cover the entire region and were also constrained in the list of TE studied.

The present study focuses on the rapidly changing oceanic region of the Barents Sea and adjacent waters of the Norwegian Sea to investigate the potential impacts of Atlantification. The aim of this work is to study the elemental composition of particulate matter in the euphotic layer and the BBL of the Barents and Norwegian Seas during the summer period, in order to identify the sources, sinks, and the relationship between trace elements and major phase composition.

2. Materials and Methods

2.1. Study Area

The studied region is located in the area of interaction between the Atlantic (AW) and Polar (PW) water masses. The Norwegian and Barents seas are highly productive and characterized by lower river discharge than the Siberian Arctic seas. The Norwegian Sea includes the continental slope and the foot of the continental slope and is characterized by depths up to 3970 m. The Barents Sea is a marginal sea of the Arctic Ocean with a depth of usually less than 300–350 m (Figure 1a).

An important factor influencing the distribution of SPM in the Norwegian Sea is the hydrological regime of the Bear Island Trough, which is a gateway for the supply of sedimentary matter from the Barents Sea [22,35,36]. The relief of the Norwegian Sea bottom also determines the existence of significant BNLs confined to the continental slope and its foot and linked to contour currents [37]. The water column is primarily represented by two water masses: The AW, which occupies the upper layer to a depth of approximately 500 m,

and the Norwegian deep water from 500 m down to the bottom [32]. The deep waters of the Norwegian Sea are not influenced by the waters of the Barents Sea in the summer.

The warm and salty AW flows into the southern part of the Barents Sea from the Norwegian Sea (Figure 1). Entering the Barents Sea as the North Cape Current, the AW is divided into two main branches [38,39]. The northern branch flows northeast along the trough of Hope Island, where it splits and passes over the threshold between the Perseus Rise and Svalbard (76.5° N), while its other part circulates in the Bear Island Trough and then comes out of the Barents Sea. The main branch of the AW in the form of the Murmansk Current extends eastward towards the Novaya Zemlya Archipelago. The Murmansk Current is a continuation of the Norwegian Coastal Current, which circles around Europe along the coastline (Figure 1a). Moreover, the AW flow in the form of subsurface water enters the Barents Sea from the Arctic Basin [40]. The relatively cold and fresh Arctic waters (ArW) enter the Barents Sea from the Arctic Basin between Svalbard and Franz Josef Land (FJL), as well as between FJL and Novaya Zemlya at layers of 0–100 m. The Barents Sea is going through a marine climate transition dubbed the *'Atlantification'* [41]. Regular satellite observations indicate annual summer blooms of coccolithophorid *Emiliania huxleyi* in the southwestern part of the Barents Sea [42–44] caused by an increase in the water temperature. Results of phytoplankton studies (including coccolithophorid blooms) during the same cruise were reported previously [45,46].

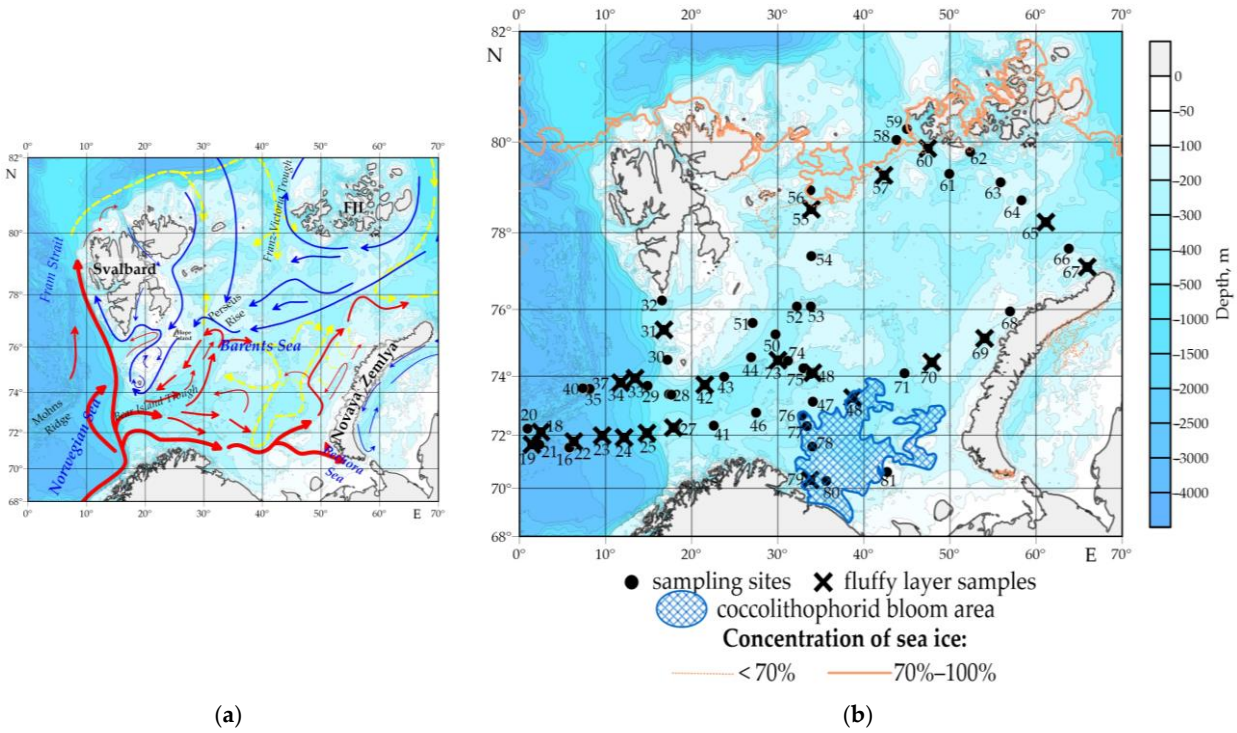

(**a**) (**b**)

Figure 1. (**a**) Water circulation scheme after [38,39]: red arrows—warm currents; blue arrows—cold currents; dashed yellow arrows—subsurface currents. (**b**) Map of SPM and FLSM sampling stations, July—August 2017. Station numbers are omitted in the first two digits. The area of coccolithophorid blooms (>1.5 106 cells/l) according to satellite data in August 2017 [44]; sea ice conditions from satellite imagery on August 8, 2017 [47]. Bathymetric data—IB-CAO [48].

2.2. Field Observations and Sample Collection

SPM samples from the Norwegian and Barents seas were collected during the 68th cruise of the RV Akademik Mstislav Keldysh in July–August 2017 (Figure 1) [49]. The sampling layers were selected based on preliminary hydrophysical and hydro-optical profiling data. SBE9p probing system was used, including 10-L Niskin water bottles (24 pcs) and a CTD-probe SBE 9+ with temperature, conductivity, pressure, and oxygen gauges. Vertical profiles

of the temperature and salinity values were built along the the sublongitudinal transect [50]. Twenty-two above-bottom water samples (0.03–0.1 m from the bottom) and FLSM were collected using a KUM multicorer.

A set of optical instruments [42] including a Ramses hyperspectral radiometer, a BIC four-channel illuminance meter, and a PHAR LI-192 LiCOR complex based on photodiode sensors were used to measure photosynthetically available radiation (PAR) at the sea surface and underwater in visible light in the spectral range of 400–700 nm. The optical measurements of the PAR profiles were carried out only during daylight time. The obtained underwater PAR profiles made it possible to calculate the depth of the euphotic layer.

To study the mass concentration of SPM and its elemental composition, SPM was extracted by means of vacuum filtration through preweighed (with an accuracy of ±0.01 mg) nuclear membrane filters with a diameter of 47 mm and a pore size of 0.45 µm produced by the Joint Institute for Nuclear Research (Dubna, Russia). Before use, the filters were washed with a 1N HCl solution at room temperature for ~24 h and then washed repeatedly with deionized water to achieve normal pH (~5.5). In parallel, SPM was collected on fiberglass filters Whatman GF/F 47 mm in diameter to determine the total and organic carbon (TC and TOC). Before use, the filters were calcined at 450°C for 4 h. The BBL was assumed to be 50 m from the bottom in further measurements. Above-bottom water samples were treated according to the same procedure as the samples from Niskin water bottles to collect FLSM.

2.3. Determination of Major Particulate Phases

The contents of TC and TOC were determined by automatic coulometric titration (Table 1) using an AN-7529 device (Russia). TOC was determined after washing the filter with a hydrochloric acid solution, and TC was determined on an untreated filter. The accuracy of the analysis is 5% when TC content is less than 20%. The content of organic matter (OM) was calculated by multiplying TOC by 2 [51]. Total inorganic carbon (TIC) content was calculated by subtracting TOC from TC. From the TIC content, the calcium carbonate $CaCO_3$ was calculated using the stoichiometric coefficient.

Table 1. Chemical analytical methods and total number of SPM samples analyzed.

Method	Measured Value	Number of Stations Studied	Number of Samples Analyzed
Coulometric titration	TC, TOC	20	78
Photocolorimetry	Si, Al, P	20	78
ICP-MS	Mn, Ti, V, Co, Ni, Cu, Rb, Sr, Cd, Ba, La, Ce, Pb, U	65	295
FAAS	Fe		

Total particulate Si (totSi), Al, and P were determined using the photometric method with a UNIKO 1201 device (Russia). The sample was fused previously in a muffle furnace (at a temperature of 350 °C for 4 h) with a mixture of Na_2CO_3 and $Na_2B_4O_7$ and the addition of KNO_3. The fusion was dissolved in 3M HCl [52]. The standard reference matter (SRM) of ocean sediments (OOPE-101 and OOPE-401, Russia) was used to assess the quality of the analysis. The discrepancies with the SRM passport values of the contents of the measured elements in SRM were 2%–5%. The content of lithogenic matter (LM) was calculated by multiplying the Al by a factor of 11.6 based on the average aluminum content in the Earth's crust [53]. The silicon content exceeding the lithogenic content estimated by the Si/Al ratio in the upper continental crust [53] was calculated as exSi. The Si enrichment of SPM relative to lithogenic matter is usually explained by the presence of biogenic amorphous silica [54].

2.4. Elemental Analyses of Particulate Matter

The elemental analysis of SPM was performed through inductively coupled plasma mass spectrometry (ICP-MS) using the Agilent 7500a quadrupole instrument (USA) and

flame atomic absorption spectrometry (FAAS) using the "KVANT-2A" instrument (Kortek, Russia). Filters with the weighed SPM were placed in Teflon (Savillex™) vials, filled with a mixture of nitric and hydrogen peroxide ultrapure concentrated acids, and placed in an ultrasonic bath for 90 min at a temperature of 70 °C. After cooling, the filters were removed from the vials and washed with a small amount of 0.1 N nitric acid. Then the samples were brought to a volume of 20 mL with deionized water. A multi-element standard curve containing 10 ppb of indium was used to calculate trace element concentrations after the subtraction of the instrument blank. Digest blanks were subtracted from the sample and filter blanks were adjusted for a blank derived from the digestion acids and Teflon vials. The overall analytical precision was 5%–10% based on five replicate analyses of a single sample digest solution.

The accuracy of the analysis was ensured by using the standard reference material (SRM), namely, GSD-2 and GSD-6 composed of stream sediment powder (Institute of Geophysical and Geochemical Exploration, China). A weighed portion of a standard sample (7–10 mg) was placed in a vial together with a blank filter and subjected to the same procedures as the samples. The analysis was conducted using replicates, blanks, field blanks, and SRMs in order to maintain standard quality.

The determination of iron was carried out by FAAS. The accuracy of the method based on the measurement of a standard sample was 5%–7%. The remaining elements (Mn, Ti, V, Cr, Co, Ni, Cu, Rb, Sr, Cd, Ba, La, Ce, Pb, and U) were determined by ICP-MS. The accuracy of the method estimated on the basis of measurements of standard samples was 10%–20% depending on the element.

The statistical analysis was performed using the Statistica7 software. Ward's hierarchical cluster analysis identifies groups of elements with similar distribution patterns. This method performs sequential joining of elements in clusters on the basis of correlation between every pair of elements. A value equal to "1–Pearson R", where "Pearson R" is the Pearson correlation coefficient, was used as a linkage distance.

3. Results

3.1. Hydrological Conditions

In the studied part of the Norwegian Sea, the salinity averaged 34.9–35.1 psu. In the eastern part of the sea, the upper layer of the 0–50 m water column was fresher, with the salinity ranging from 34.4 to 34.9 psu in the area from the Scandinavian Peninsula to the Bear Island Trough (Figure 2; Table S1).

The water temperature in the upper 300–500 m layer of the deep sea was positive, decreasing with depth from 9.7 °C to zero values and reaching negative values to –0.8 °C near the bottom. The thickness of the layer of positive temperatures increased eastward from the Mohns Ridge to the continental slope. In the eastern part of the sea at a depth of less than 1000 m, the temperature of the water column was positive from the surface to the bottom. In the bottom layer, the water temperature varied from 3.3 to 6.6 °C, reaching the highest levels in the coastal Norwegian Current.

The average temperature and salinity of the upper layer of the transformed AW entering the western part of the Barents Sea to a depth of 50–60 m was 10.5 °C and 35.0 psu, respectively. In the deepwater layer (deeper than 70 m), the AW characteristics changed to 6.0 °C and 35.1 psu.

In the northern and northeastern parts of the Barents Sea, where the ArW comes in, the average characteristics of the upper (50–60 m) and lower (>70 m) water masses were as follows: –0.7 °C, 34.7 psu and –1.5 °C, 34.5 psu, respectively. The Barents Sea water, which is formed in the sea itself as a result of AW transformation under the influence of local conditions, occupied the central part of the sea, and its average water temperature and salinity were 4.0 °C and 35.0 psu, respectively.

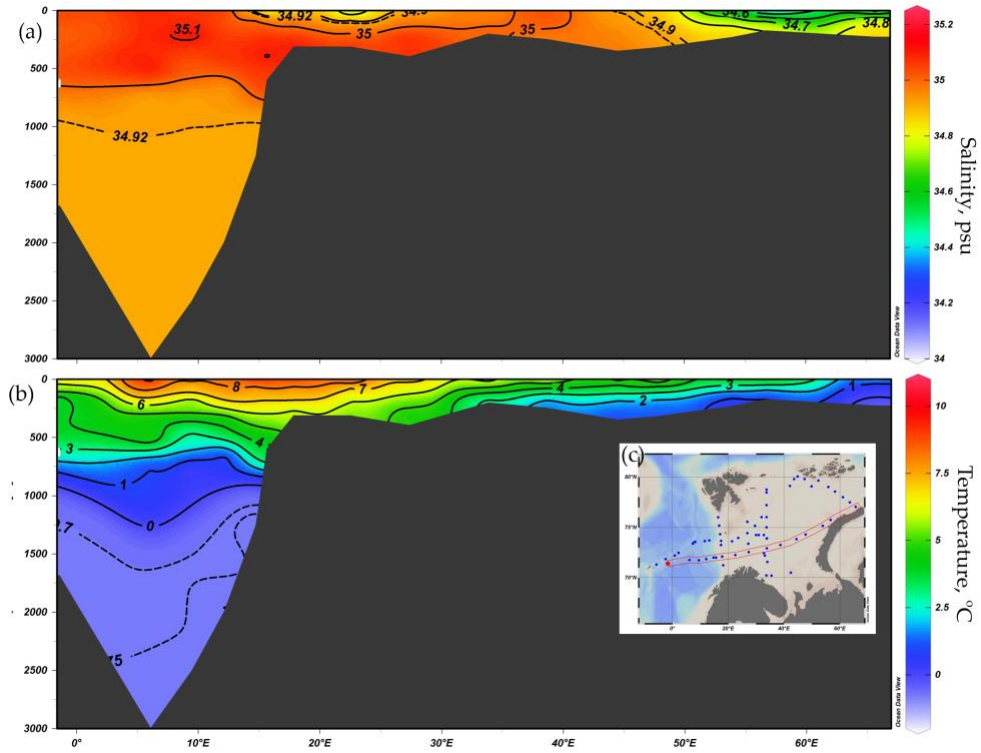

Figure 2. Vertical profiles of temperature (**a**) and salinity (**b**) along the transect (**c**).

The depth of the euphotic layer is defined as the depth where the descending PAR is 1% of the surface values. The depth of the photic layer in the study area of the Norwegian and Barents seas ranged from 24 to 46 m and from 12 to 51 m, respectively (Table 2). The narrow euphotic layer of fewer than 18 m was observed in the Barents Sea south of 72°27′ N within the area of the coccolitophorid bloom (stations 5576–5580). The daily PAR exposure on the surface of the Barents Sea ranged from 18 to 37 Einsteins m^{-2} day^{-1} and depended on cloud cover. The thickness of the euphotic layer in the southern part of the Barents Sea decreased 2–4 times compared to the northern and eastern regions of the sea, where coccolithophorid blooms were absent. The greatest depth of the photic layer (51 m) was observed at stations 5555 and 5566 in the northern and northwestern regions of the Barents Sea (both stations are located north of 77° N).

3.2. Concentration of SPM

The concentration of SPM in the euphotic layer of the Norwegian Sea ranged from 0.1 to 0.7 mg/L (Table S1), averaging 0.35 ± 0.12 mg/L (n = 37). In the intermediate water layer, the SPM concentrations are generally the lowest, ranging from 0.04 to 0.07 mg/L. The SPM concentration in the BNL ranges from 0.05 to 0.8 mg/L, averaging 0.13 ± 0.14 mg/L (n = 27). There is no BNL within the Mohns Ridge area, and SPM concentrations near the bottom correspond to those in the intermediate water column (0.04–0.08 mg/L).

The concentration of SPM in the euphotic layer of the Barents Sea ranged from 0.1 to 2.7 mg/L (Table S1), averaging 0.53 ± 0.48 mg/L (n = 72). From the lower boundary of the thermocline to the BBL, SPM concentrations were the lowest, ranging from 0.04 to 0.1 mg/L. Within the BBL, the bottom BNL and FLSM are usually distinguished. The concentration of SPM in the BNL ranges from 0.1 to 0.8 mg/L, averaging 0.31 ± 0.18 mg/L (n = 40).

Table 2. Depth of euphotic layer (PAR 400–700 nm of 1%) at the stations in the Norwegian and Barents seas.

Station	DD/MM/YY	Depth of Euphotic Layer, m
	Norwegian Sea	
5516	19/07/2017	31
5521	21/07/2017	41
5523	22/07/2017	24
5525	23/07/2017	26
5528	24/07/2017	46
5531	25/07/2017	38
5533	26/07/2017	28
5535	27/07/2017	36
5540	29/07/2017	31
	Barents Sea	
5542	30/07/2017	44
5548	01/08/2017	20
5550	02/08/2017	18
5553	03/08/2017	38
5555	04/08/2017	51
5556	04/08/2017	25
5557	05/08/2017	48
5557A	07/08/2017	43
5563	08/08/2017	32
5566	09/08/2017	51
5568	10/08/2017	24
5570	11/08/2017	36
5572	12/08/2017	29
5573	13/08/2017	34
5574	13/08/2017	23
5576	14/08/2017	18
5577	14/08/2017	15
5580	15/08/2017	12

3.3. Major Phase Composition of SPM

The OM in SPM varies from 8.3% to over 95%, while the $CaCO_3$ varies from 5.6% to 90% (Table S2). The average contents of OM and $CaCO_3$ in the euphotic layer of the Norwegian Sea are 67% ± 25% and 25% ± 27%, respectively. The highest $CaCO_3$ contents (exceeding 65%) were observed at stations 5525 and 5530. $CaCO_3$ in the BBL of the Norwegian Sea is similar—the average content is 24% ± 25%, while OM in the BBL is lower than that in the euphotic layer and the average content is 48% ± 30%.

The OM in both the euphotic layer and BBL of the Barents Sea is lower; its average content is 38% ± 28% and 33% ± 18%, respectively. In contrast, $CaCO_3$ content in the euphotic layer of the Barents Sea is higher at 55% ± 34%, while $CaCO_3$ in the BBL is approximately 3 times lower than in the euphotic layer. The peak values of $CaCO_3$ are reached at stations 5576–5580, 5548, and 5573. At the same stations, the OM content is lower than in the entire dataset.

Si content in SPM varies from 0.02% to 27.0%, Al content varies from 0.01% to 8%, and P content varies from 0.06% to 0.66%. The average contents of these elements in the euphotic layer of the Norwegian Sea are 2.6% ± 1.2%, 0.37% ± 0.34%, and 0.32% ± 0.17%, respectively. Those contents in the BBL of the Norwegian Sea are 8.6% ± 4.8%, 1.74% ± 1.30%, and 0.17% ± 0.08%, respectively.

The average Si, Al, and P contents in the euphotic layer of the Barents Sea are 2.6% ± 4.7%, 0.19% ± 0.20%, and 0.34% ± 0.15%, respectively, and those contents in the BBL are 14.1% ± 7.8%, 4.0% ± 2.9%, and 0.21% ± 0.07%, respectively. The highest Si content (21.7%) is observed at the 30 m layer of station 5561. The distribution of the major phase in SPM is heterogeneous, with a higher variation in the SPM in the euphotic layer.

3.4. Elemental Composition of SPM

The elemental composition of the SPM is quite variable, especially in the euphotic layer (Table S1). Average TE contents in different areas in the euphotic, intermediate layer, and BBL are shown in Table 3. The most abundant TEs in the SPM of the euphotic layer are Mn, Fe, Ti, Sr, and Ba (in order of decreasing content) and those of the BBL are Fe, Mn, Ti, Ba, and Sr. Most elements show higher concentrations in the BBL compared to the euphotic layer. The exceptions are Sr, Cu, Cd, and U, as their contents are considerably higher in the euphotic or intermediate layer. The spatial distributions of some of the TEs in the SPM of the surface (2–10 m) layers and BBL are shown in Figure 3a–h.

Table 3. Element content in SPM of euphotic layer (1), intermediate layer (2), and BBL (approximately 50 m from the bottom) (3). Standard deviation values are indicated in the brackets.

	Fe (%)	Mn (%)	Ti (ppm)	V (ppm)	Co (ppm)	Ni (ppm)	Cu (ppm)	Rb (ppm)	Sr (ppm)	Cd (ppm)	Ba (ppm)	La (ppm)	Ce (ppm)	Pb (ppm)	U (ppm)
the Norwegian Sea (15 stations)															
1	0.06	0.19	137.6	7.28	2.42	10.46	89.5	3.06	278	5.19	155	2.15	4.16	8.98	5.50
	(0.05)	(0.09)	(89.1)	(4.31)	(0.84)	(6.32)	(67.3)	(1.16)	(185)	(2.08)	(235)	(2.70)	(6.56)	(9.25)	(4.23)
2	0.47	0.29	1307	23.97	6.27	19.15	127.9	12.59	313	2.34	574	10.67	23.92	33.58	2.72
	(0.34)	(0.09)	(1168)	(13.14)	(2.63)	(12.21)	(54.1)	(11.86)	(119)	(1.89)	(238)	(8.47)	(16.49)	(18.37)	(2.48)
3	0.99	0.36	1472	39.18	9.67	24.86	158.8	21.54	340	3.88	558	12.37	28.83	65.11	1.80
	(0.39)	(0.12)	(1383)	(20.34)	(3.99)	(8.62)	(134.6)	(16.22)	(140)	(8.84)	(184)	(5.50)	(12.87)	(64.03)	(1.16)
Bear Island Trough (6 stations)															
1	0.06	0.11	–	8.89	1.72	6.53	67.3	9.47	364	4.32	278	3.65	9.32	8.71	1.75
	(0.09)	(0.06)		(7.60)	(0.86)	(6.29)	(57.9)	(10.17)	(271)	(1.83)	(481)	(6.23)	(15.92)	(9.89)	(1.61)
2	0.36	0.19	1014	24.08	4.12	10.16	76.6	11.31	216	2.07	235	7.60	16.06	22.27	1.39
	(0.15)	(0.04)	(186)	(7.14)	(1.49)	(6.71)	(37.3)	(7.65)	(53.8)	(1.30)	(163)	(2.49)	(5.86)	(6.95)	(0.50)
3	1.35	0.24	1964	87.01	8.49	21.68	42.3	48.46	222	1.35	322	18.01	41.89	27.86	1.59
	(0.30)	(0.05)	(624)	(31.77)	(1.87)	(6.43)	(15.6)	(14.82)	(83.9)	(0.48)	(130)	(2.96)	(7.54)	(5.33)	(1.06)
the Barents Sea shelf proper (24 stations)															
1	0.09	0.18	472	27.2	2.37	13.88	140.3	8.90	250	3.30	349	3.96	8.17	14.02	2.37
	(0.14)	(0.15)	(376)	(34.4)	(1.78)	(20.6)	(132.5)	(9.96)	(219)	(1.91)	(584)	(10.52)	(19.61)	(11.89)	(2.61)
2	1.06	0.59	1349	123.7	10.95	37.02	252	56.12	355	5.60	848	22.88	43.89	46.73	2.03
	(0.82)	(0.46)	(1214)	(83.6)	(8.64)	(23.5)	(211)	(80.65)	(263)	(3.04)	(756)	(34.30)	(47.33)	(23.64)	(1.31)
3	1.61	0.48	1970	186.3	11.15	25.98	92.9	62.85	251	2.60	553	19.54	44.86	30.32	1.55
	(0.80)	(0.41)	(1126)	(118.5)	(6.14)	(15.3)	(64.9)	(42.96)	(105)	(1.31)	(344)	(7.18)	(16.48)	(11.14)	(0.74)
Area of coccolithophorid bloom in the southern Barents Sea (5 stations)															
1	0.05	0.06	35	1.6	1.31	6.3	24.2	6.47	238	2.56	262	5.02	10.67	19.26	1.90
	(0.04)	(0.04)	(31)	(1.3)	(1.21)	(5.39)	(21.1)	(5.76)	(163)	(1.71)	(335)	(6.28)	(14.29)	(13.29)	(1.81)
2	0.41	0.20	328	18.0	4.9	16.0	46.1	18.12	186	3.22	404	9.06	21.89	32.40	1.84
	(0.31)	(0.06)	(125)	(9.6)	(1.3)	(9.5)	(35.4)	(12.05)	(116)	(1.21)	(371)	(3.78)	(9.36)	(20.34)	(1.43)
3	1.45	0.17	610	40.6	7.6	22.2	36.8	53.40	219	2.60	554	18.31	43.11	31.94	2.00
	(0.91)	(0.10)	(358)	(32.6)	(4.18)	(10.82)	(13.2)	(28.16)	(58)	(1.17)	(388)	(5.72)	(12.93)	(9.79)	(0.94)

3.5. FLSM Compostion

The elemental composition of the FLSM shows a more uniform spatial distribution (Table S3) compared to the SPM of the upper layers of the water column. Average OM and $CaCO_3$ contents in the FLSM of the Norwegian Sea are 15.8% ± 10.8% and 30.6% ± 37.8%, respectively. Average OM and $CaCO_3$ contents in the FLSM of the Barents Sea are lower than those of the Norwegian Sea at 3.2% ± 3.4% and 3.5% ± 1.8%, respectively. Si, Al, and P contents in the FLSM of the Norwegian Sea are 12.1% ± 6.3%, 5.1% ± 2.9%, and 0.11% ± 0.01%, respectively, and those of the Barents Sea are 25% ± 2.6%, 7.5% ± 0.4, and 0.18% ± 0.07%. The most abundant TEs in the FLSM are Fe (2.1% ± 0.8%), Ti (0.52% ± 0.19%), Mn (0.21% ± 0.08%), Sr (554 ± 242 μg/g), and Ba (343 ± 98 μg/g) in the Norwegian Sea, and Fe (2.6% ± 1.4%), Mn (0.36% ± 0.54%), Ti (0.23% ± 0.16%), Sr (282 ± 196 μg/g), and Ba (257 ± 109 μg/g) in the Barents Sea. A comparison of the SPM in the BNL with that in the FLSM shows the similarity of their elemental composition (Tables S1–S3).

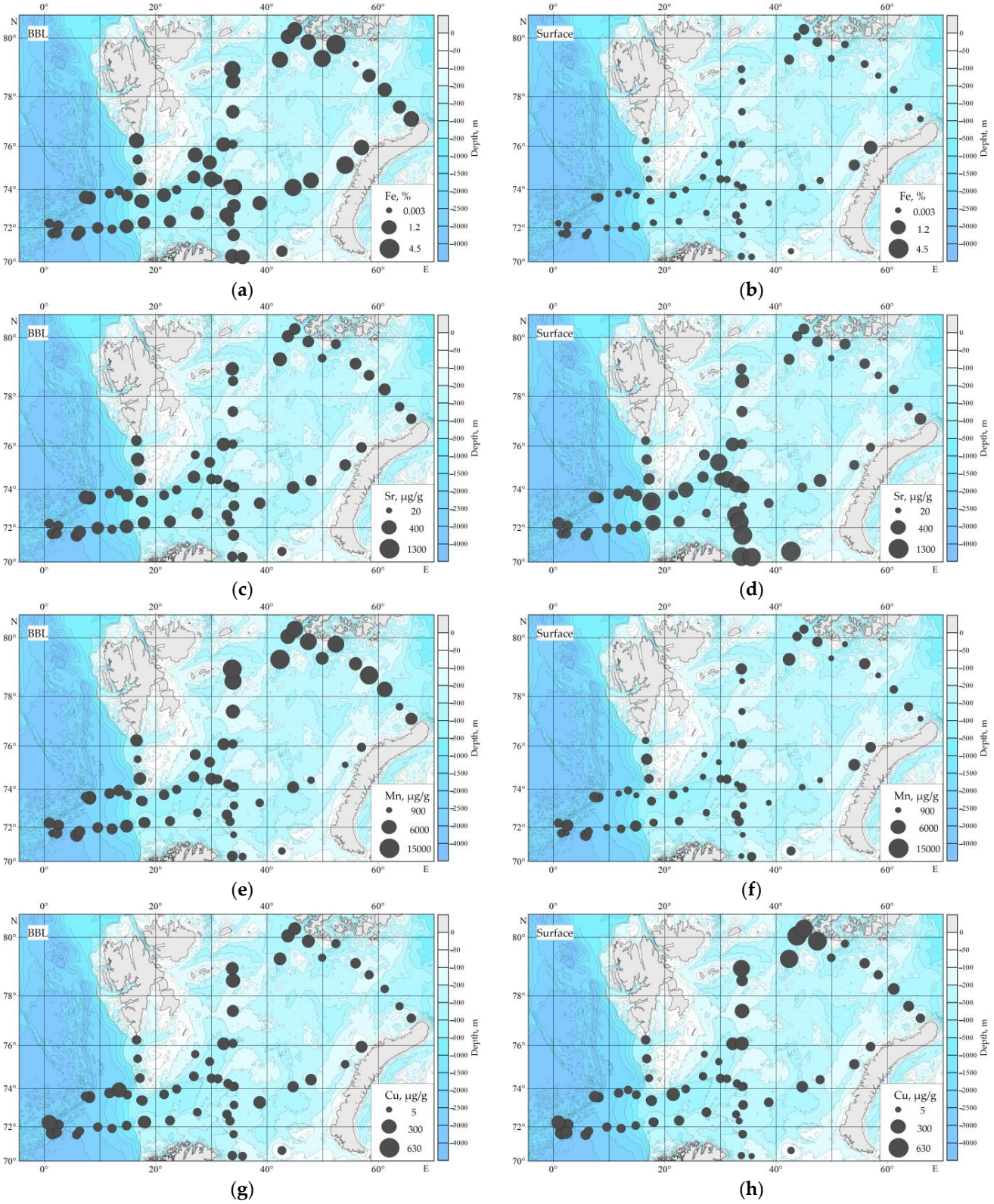

Figure 3. Spatial distribution of TEs: Fe (**a**,**b**); Sr (**c**,**d**); Mn (**e**,**f**); Cu (**g**,**h**) in the SPM of the surface (2–10 m) layer and BBL.

4. Discussion

4.1. SPM Distribution in the Euphotic Layer

The assessment of solar radiation penetration within the 400–700 nm spectral range (PAR) into the waters of the Arctic seas is important, first of all, as a factor determining the primary production of phytoplankton, and hence the biogenic SPM in the euphotic layer of the water. Cloud cover has been proven to be the main factor affecting the incoming PAR: For the same PAR value at the upper boundary of the atmosphere (approximately 56 Einsteins $m^{-2}day^{-1}$), the values of daytime exposure on the sea surface varied, depending on cloud cover, almost by a factor of 5, from less than 10 to 45 Einsteins-$m^{-2}day^{-1}$ [55]. The thickness of the euphotic layer, where active biogeochemical processes occur, is determined primarily by the content of optically active components such as SPM and colored dissolved organic matter in the seawater [56,57]. The thickness of the euphotic layer in the Barents Sea varied over a wider range compared to that in the Norwegian Sea, reaching the lowest thickness in the area of coccolithophorid bloom (stations 5576–5580). Coccolithophorids and detached coccoliths are major factors in the scattering of solar radiation and increase the albedo of water significantly [55]. In August 2017, the albedo was less than 1% in the areas where no blooming was observed and increased to 12% at station 5580 where coccolithophorid concentrations in the surface (2–10 m) layer were as high as 5.3×10^6 cells L^{-1}. The SPM concentration at the stations with coccolithophorid blooming was the highest (from 0.7 to 2.3 mg/L) in the upper layer of 5–20 m. This population of coccolithophorid *Emiliania huxleyi* is suggested to be of "Atlantic" origin [46], and the increased frequency and area of coccolithophore blooms within the Barents Sea were triggered by the increased influence of the AW over the last two decades [58].

The highest SPM concentrations in the Barents and Norwegian seas are usually confined to phytoplankton bloom areas. Various seasonal cycles of phytoplankton in July-August were revealed, such as the massive development of the Arctic diatom species in the north of the Barents Sea near the marginal ice zone (MIZ) from 78°46′ to 80°03′ N and the explosive growth of autotrophic boreal dinoflagellates in the area of the Polar Front [59]. The accumulations of the phytoplankton biomass corresponded to the high chlorophyll "a" concentrations of up to 5 µg/l [60]. In the southern area of the Polar Front in the Barents Sea, the SPM concentrations reached 0.7–1.0 mg/L in the surface layer of 5–20 m due to increased blooming of boreal dinoflagellates [59]. In the MIZ of the Barents Sea, the highest SPM concentrations (0.6–0.7 mg/L) were confined to the subsurface layer of 20–45 m, i.e., to the lower boundary of the euphotic layer, where an accumulation of Arctic diatom species occurred [59].

The spatial distribution of SPM in the euphotic water layer of the Barents Sea is rather mosaic but generally in line with the circumcontinental zonality [1]. There is a regular decrease in the SPM concentration further away from the seacoast. The distribution of SPM in the open part of the sea is governed by seasonal succession patterns of phytoplankton, which vary considerably within the Barents Sea. The SPM concentrations in the euphotic layer range from 0.1 to 1.2 mg/L, which is consistent with the data obtained for the Barents Sea in the 1990s. [25]. The concentration ranges in the uppermost sea layer have not changed, but the areas of the elevated SPM concentrations in the southern parts of the sea have expanded and are associated with extensive coccolithophorid blooming. The areas of increased SPM concentrations confined to the Polar Front shifted northward in the last two decades. An increase in terrigenous particle flow from the archipelagos associated with glacier melting is expected [61].

In the Norwegian Sea, elevated SPM concentrations (0.4–0.6 mg/L) in the surface (2–10 m) layer were observed in the southern part of the Bear Island Trough fan at a depth drop of approximately 300 to 2900 m (stations 5522–5527), where water temperatures reach 9.6–10.5 °C. SPM concentrations ranged from 0.2 to 0.4 mg/L in the Arctic Front area in the southernmost Mohns Ridge, mainly due to biogenic particles such as diatoms, haptophytes, etc. [45]. The highest concentrations of up to 0.5–0.7 mg/L in the euphotic layer with a

surface water temperature under 7 °C were found in the eastern part of the sea from Bear Island to Svalbard at a depth of approximately 200–350 m.

4.2. SPM Vertical Distribution and Major Phase Composition

The vertical distribution of the SPM concentration demonstrates extremes in the euphotic layer and BNL and low concentrations in the intermediate water layer between the lower boundary of the thermocline and the upper boundary of the BBL. The vertical distribution of the major phases (OM, $CaCO_3$, lithogenic matter, and $exSiO_2$ as a proxy of bSi) in SPM is shown in Figure 4. The contribution of lithogenic material increases with depth at all stations (Figure 4) due to the resuspension of sediments [23].

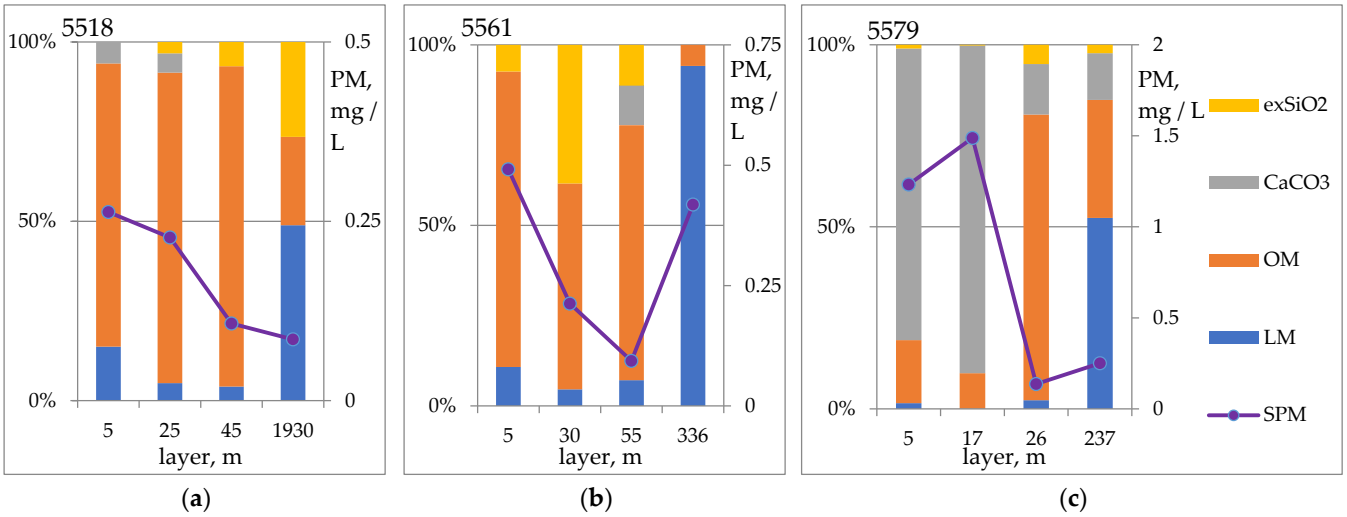

Figure 4. Vertical distribution of major phase and concentration of the SPM at stations (**a**) St. 5518, (**b**) St. 5561, and (**c**) St. 5579. SPM concentrations are plotted along the secondary axis.

The distribution of the major phase is largely governed by biological processes on the one hand and by the inflow of terrigenous material on the other. Thus, an increase in the $CaCO_3$ is observed in the euphotic layer of stations showing blooming of coccolithophorids *E. Huxleyi* and *C. Pelagicus* at stations 5576–5581, 5527, and at the periphery of these areas (5548, 5525), where coccolithophorid bloom was also observed on a smaller scale. The maximum content of $CaCO_3$ at these stations is observed in the zone of coccolithophorid occurrence in the upper 20 m of the water column (Figure 4c) [43,45]. Beyond these areas, $CaCO_3$ is uniformly distributed, decreasing in areas of terrigenous runoff and dominance of other phytoplankton species. Station 5561, located in the MIZ, is expected to be enriched in $exSiO_2$ at the 30 m layer, the area of maximum abundance of ice diatom species [59].

OM in the euphotic layer shows a decrease in concentrations in the coccolitophorid blooming area and is more uniform beyond it since the OM content in that phytoplankton is low [48]. OM in the SPM of BBL is relatively uniform but decreases in the south of the Barents Sea, evidently because of the lower content of OM in bottom sediments there [62].

In the Barents Sea, BNLs are much less common and have a lower thickness and lower concentrations of SPM compared to the Siberian Arctic seas [63,64]. Nevertheless, the recent prolongation of the open-water season causes higher sediment resuspension and coastal erosion due to larger wind fetches and wave heights [30]. This impacts the optical properties of the water column and, hence, the biological productivity in this region. The thickness of BNL in the Barents Sea is approximately 20 m and the concentration of SPM can reach 0.8 mg/L (St. 5569—the West Novaya Zemlya Trough). Intense BNLs with an SPM concentration of up to 0.4–0.6 mg/d were confined to the region located between the FJL and Novaya Zemlya Archipelagos (stations 5562–5565). This area is influenced by two water masses, namely, mixed ArW and AW, and also PW of Arctic origin [65] entering from the northeast to the Barents Sea. The reduction of seasonal ice cover over a large area of

the Barents Sea following the recent "Atlantification" may lead to an increase in the winter convection and resuspension of sediments [30].

In the studied area of the Norwegian Sea, the BNLs with an SPM concentration of up to 0.8 mg/L were observed in the Svalbard region (stations 5529–5531). In the rest of the sea, BNLs were weak (0.1–0.2 mg/L) or almost absent in the southernmost segment of the Mohns Ridge. Intermediate NLs were observed in the area of hydrothermal plumes' influence in the vent fields of the Mohns Ridge [16,66].

4.3. Correlations between TE and Major Phases of SPM

As it was shown [54], all the elements in SPM tend to accumulate a certain major phase. To determine the carrier matrix for different elements, correlation analysis with clustering of variables was performed separately for the Norwegian and Barents seas (Figure 5a,b).

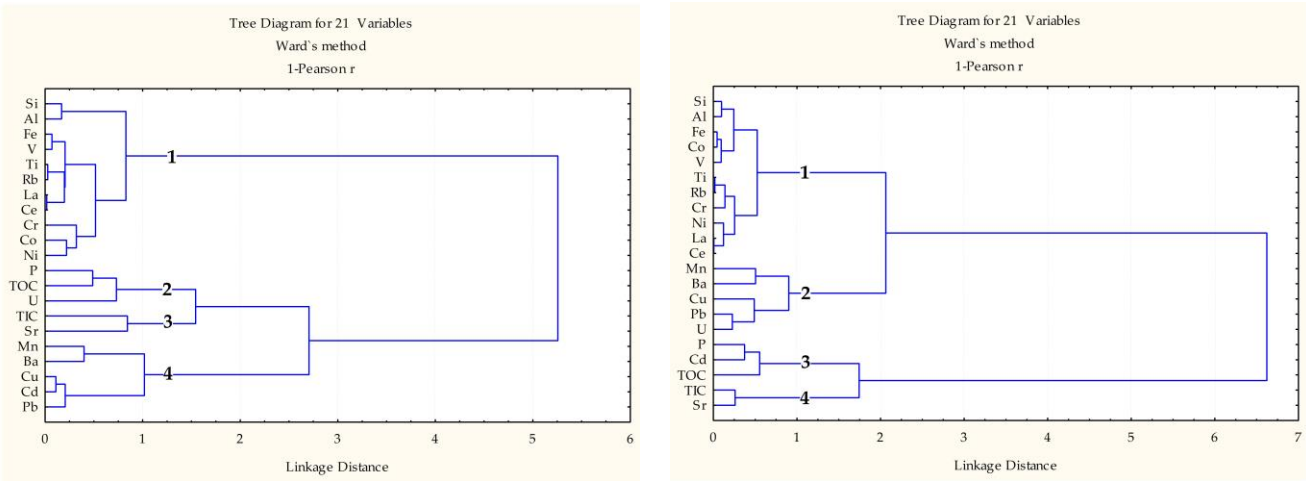

(**a**) (**b**)

Figure 5. Cluster tree diagram for elements and major phase in the SPM of (**a**) the Norwegian Sea and (**b**) the Barents Sea.

For both seas, four groups of elements are distinguished, three of which are interpreted as related to a particular phase of SPM. The first group includes Si, Al, Fe, V, Ti, Rb, Cr, La, Ce, Co, and Ni. These elements have an affinity to the lithogenic matter, as evidenced by high correlation coefficients with aluminum ranging from 0.40 (for Ti) to 0.83 (for Fe and Si) (Figure 6a,b). Some diatom algal communities in the Arctic tend to accumulate aluminum [67]. While the proportion of biogenic silica in marine SPM is usually significant, Si seems to have been assigned to the lithogenic group in our samples. The sample characterized by the maximum diatom algae content at st. 5561 [59] stands out from the line of regression (Figure 6b). Note that the correlation between Si and Al in the upper 40 m of the water column is weaker than that at depths greater than 50 m (0.33 and 0.91, respectively). Elements of this group show a gradual increase in content with depth as the proportion of the lithogenic matter increases too. For example, the correlation coefficients between the iron content in SPM and the depth of the sampling horizon are 0.80 and 0.76 in the Norwegian and Barents seas, respectively (Figure 6c).

The second group of elements are those with affinity to OM; they include P and TOC, which is expected because phosphorus is one of the main nutrients in the ocean [68]. In the Norwegian Sea, this group is joined by U, and in the Barents Sea by Cd (Figure 4a,b). Although Cd is a highly toxic element [69], it is assimilated by living organisms [70] and is included in the extended Redfield Ratio [71]. Similar behavior of cadmium and phosphorus in the water column during the formation and remineralization of organic matter has been noted in many studies [13,72] The behavior of uranium during sedimentation is generally quite conservative, but excess uranium formed in the euphotic water layer is widespread [73,74]. Studies have shown that excess uranium is completely regenerated

before particles are buried in sediments in the oxygenated open ocean. Elements of the second group reach their maximum in the subsurface or surface horizons and decrease with depth as the organic matter is remineralized.

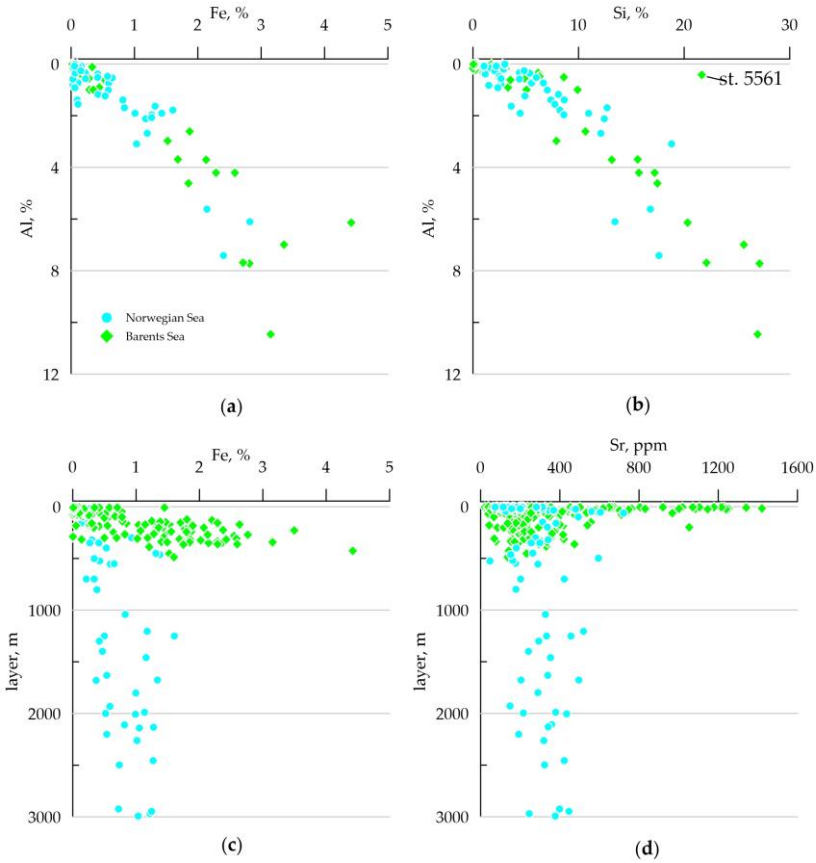

Figure 6. Scattering diagrams between (**a**) Al and Fe; (**b**) Al and Si; (**c**) depth of sampling and Fe; (**d**) depth of sampling and Sr.

The third group is Sr—a bioessential trace element with affinity to carbonate matter. Sr shows a positive correlation coefficient with TIC content (0.63) for the whole set of samples, and its content in SPM is governed by biogenic $CaCO_3$. The correlation between Sr and TIC in the Norwegian Sea is much weaker than that in the Barents Sea (0.29 and 0.80, respectively). We attribute this to the difference in species composition of carbonate organisms in these seas—primarily *Coccolithus pelagicus* in the Norwegian Sea and *Emeliania huxleyi* in the Barents Sea [45]. The vertical distribution of bioessential TE (related to organic and carbonate matter) in the water column is not monotonic; the highest contents are observed at different layers within the euphotic layer.

The behavior of these elements is governed by biological processes that exhibit significant spatial and temporal variability (including diurnal cycles). This is the so-called nutrient-type distribution of TE, which is significantly involved in the internal cycles of biologically derived particulate material. Their distributions are dominated by the internal cycle of accumulation of the bulk of this material by plankton in the euphotic waters and its oxidation and remineralization in deeper waters during SPM sinking [69]. The highest content of bioessential elements is related to the upper 50–100 m, while the dispersion of the content of these elements in the upper horizons is high and decreases sharply below the thermocline (Figure 7a–i).

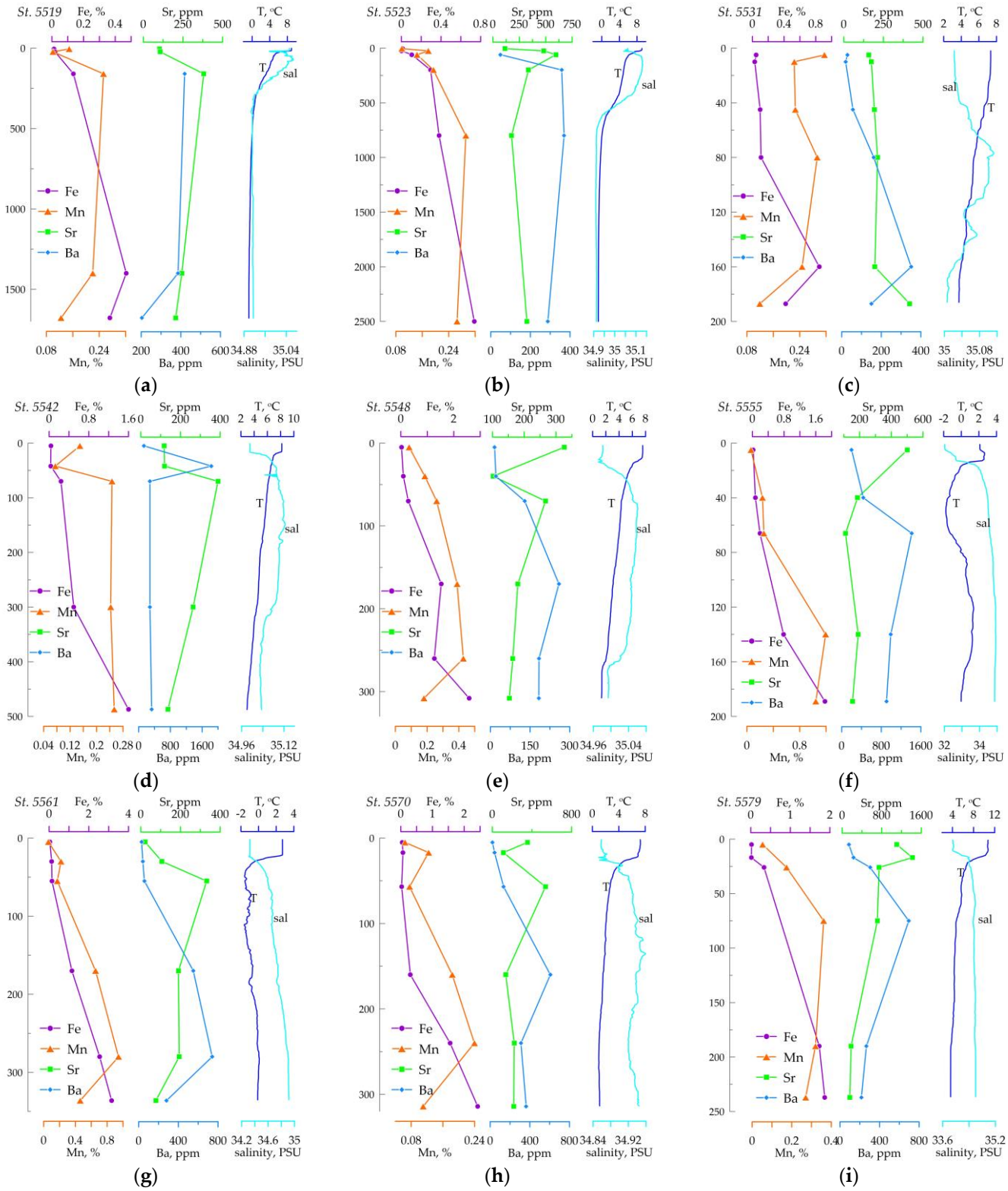

Figure 7. Vertical distribution of element contents and CTD data on temperature and salinity by depth in different stations of the Norwegian Sea (**a**–**c**) and the Barents Sea (**d**–**i**).

The vertical distribution of Sr in SPM differs between the Barents and Norwegian seas (Figure 6d). In the area of coccolithophorid blooming in the southern part of the Barents Sea, higher values of Sr content, a greater variance of these values, and a pronounced decrease with depth were observed (Figure 7i). Sr content in the SPM of the Norwegian

Sea is more homogeneous both in the water column and the aquatory. Sr content in coccolithophorids is largely controlled by the calcification rate [75], which in turn depends on the temperature [75,76] and the ratio of macronutrients [46]; therefore, an obvious relationship between temperature and Sr content was found (Figure 8). The highest Sr content corresponds to the high water temperature in the Barents Sea and on station 5527a in the Norwegian Sea.

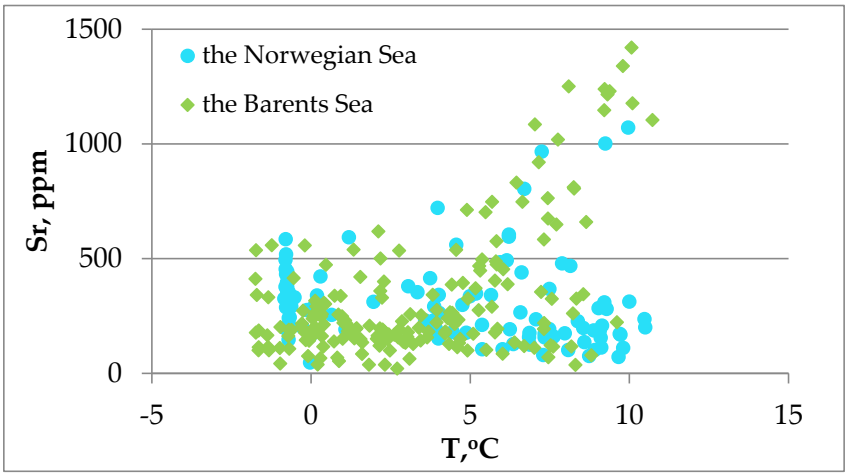

Figure 8. Relationship between temperature and strontium content.

The fourth group of elements includes Mn, Ba, Cu, and Pb. These are also accompanied by Cd (in the Norwegian Sea) and U (in the Barents Sea). Grouping of these elements into one cluster is caused by similar patterns of distribution of their contents in SPM. The distribution of Mn can be controlled by redox processes in the water column. In most cases, Mn content has two peaks—in the intermediate layer and in the euphotic layer (Figure 7). Based on the crustal ratio, the fraction of excess manganese exMn was estimated. In general, the exMn fraction decreases in the water column from 90%–99% in the upper horizons to approximately 50% in the BBL. This ambiguous behavior of particulate Mn in the water column indicates that it can be derived from hydrogenic, biogenic, and lithogenic sources. Pelagic Fe and Mn (oxyhydr)oxides that form stable crystalline phases in the SPM of the Barents Sea were revealed and described in [24]. The decisive role of bacterial activity in the formation of these minerals was demonstrated in [77]. Manganese minerals in SPM are parts of manganese recycling and are not involved in sediment or nodule formation because they are dissolved upon settling. The active formation of manganese oxides has been shown to occur in BNL due to the enrichment of benthic water with Mn from pore water [24]. Iron, while also a redox-sensitive element, is uniquely classified as a lithogenic element by the type of vertical distribution in SPM. The highest Mn content in the Barents Sea was observed in the BNL in the area between Svalbard and FJL (Sts. 5555—5561) (Figures 3e and 7f,g). In the same area, Fe-Mn crusts were described on the seafloor based on our investigations during the cruise [61], and Fe-Mn nodules were obtained by [78].

The barium cycle in the ocean is strongly associated with OM regeneration processes [79]. The vertical distribution of barium is controlled by the processes of barite formation during the decomposition of the organic matter and its further remobilization during the settling of particles [80,81]. Two peaks of barium concentrations in SPM were detected at many stations: (i) In the subsurface horizon and (ii) in the intermediate water layer (Figure 7). The direct correlation between Mn and Ba may be caused by their participation in biological processes, as well as co-precipitation on Mn-hydroxide films of bacterial cells.

Copper is assimilated by organisms [70], which aptly explains the higher copper content in the SPM of the surface water layers (Figure 3h). Moreover, the Cu content in SPM is strongly influenced by the recycling of organic matter, as well as scavenging

processes [13,70]. Therefore, copper was not considered a bioessential TE and is not correlated with TOC.

An additional source of Fe, Mn, Ba, Cu, Pb, and Cd in the Mohns Ridge area may be the submarine hydrothermal vent fields [14,66], as elevated contents of these elements were observed in the BNL and intermediate layers at stations 5516 and 5518 in the Jan Mayen vent field area, and at station 5535 close to the Troll Wall vent field (Figure 3g).

4.4. Spatial Distribution of Elements in SPM of Euphotic Layer and BBL

The spatial distribution of elements in the surface SPM shows a significant variation of values. The content of iron and lithogenic elements in the SPM of the euphotic layer of the Norwegian Sea is lower than in the Barents Sea (Table 3). There is an increase in the content of lithogenic elements in the samples collected close to shore (Figure 3a). The content of particulate lithogenic elements is higher, and their spatial distribution is more homogeneous in BNL. The SPM of the Bear Island Trough shows an intermediate level in terms of Fe content, as the AW circulates within the trough, which comes from the Norwegian Sea and partly returns. The enrichment of SPM with iron in the Barents Sea is related not only to the input of this element from the land and underlying sediments but also to pelagic iron oxyhydroxides forming stable crystalline phases in the water column, such as ferroxigite and protoferrihydrite [24]. In general, particulate Fe content in BNL tends to increase in the northeastern direction, reaching its maximum in the FJL area and the Franz-Victoria Trough. This region is also characterized by an increased particulate Mn content (Figure 3e), which may be associated with the formation of Fe-Mn oxyhydroxides [78]. Similar trends of increasing Fe content in the upper layer of the sediments of the Barents Sea were noted in [81].

The following features were revealed for the spatial distribution of Sr. Increased strontium content in the surface SPM of the southern Barents Sea associated with coccolidophorid blooms [44], as well as in the Norwegian Sea in the area of the Mohns Ridge (Figure 3c,d). Particulate Sr contents in the BNL of the Norwegian and Barents seas outside the areas of coccolidophorid bloom are at a similar level (Table 3). Particulate Sr content in BNL does not reflect its distribution in the surface layer, due to the dissolution of carbonates in the Barents Sea water column [82]. The Barents Sea is characterized by a gradual eastward decrease in Sr content in BNL, which is likely related to the carbonate matter decrease reported for the upper layer of bottom sediments [81].

4.5. Comparison of BNL SPM and FLSM Composition

The fluffy layer is distributed throughout the Barents Sea shelf. The thickness of this layer may vary from 0.5 to 1 cm, and more rarely up to 2 cm, depending on the lithological composition of the underlying sediments and hydrodynamic conditions [8]. Under calm sedimentation conditions, the thickness of the fluffy layer tends to increase. In the Norwegian Sea, the fluffy layer is found within the continental slope but is thinning and practically absent in the pelagic area. To compare the SPM composition of BNL sampled at 2–20 m from the bottom with the composition of FLSM sampled with a multicorer, the contents of the sediment were normalized to those of FLSM:

$$C_n = C_{\text{BNL SPM}} / C_{\text{FLSM}}$$

In the fluffy layer, sedimentary matter transforms from a dispersed form into a bound one, and as a result, forms a new material—marine sediment. This is the upper flocculated layer above the sediment, consisting of particles of pelitic and silty-pelitic grain size and having a water content of more than or equal to 90%. FLSM is formed as a result of sediment resuspension and settling particles from the overlying water layer and it is enriched with newly formed (microbial) organic matter [8].

For the majority of elements, a C_n value ≤ 1.2 is common, which indicates the similarity of SPM and FLSM elemental compositions; low values of C_n (less than 0.5–0.7) indicate the depletion of SPM in BNL relative to FLSM. Such depletion can be partly caused by

the dilution of lithogenic material with organic matter. The organic carbon content in the FLSM of the Norwegian Sea varies from 1.8% to 8.6%, and in the SPM of the bottom water layer, it varies from 3.1% to 3.5%. For the Barents Sea, the content of organic carbon in FLSM ranges from 1.7% to 3.3%, and in the bottom water layer SPM, from 10.1% to 11.0%. Thus, the content of organic carbon in the SPM of BNL is higher than that in FLSM (excluding St. 5531 in the Norwegian Sea with higher content of organic carbon in FLSM). Mn, Cu, Cd, Cu, and Ba are characterized by an enrichment of SPM in BNL relative to FLSM (Figure 9). It has been discussed above that these elements undergo active recycling during particle settling [13,70,79] and are characterized by an affinity to organic matter. Manganese enrichment is determined by changes in redox conditions at the water–sediment interface [24,83].

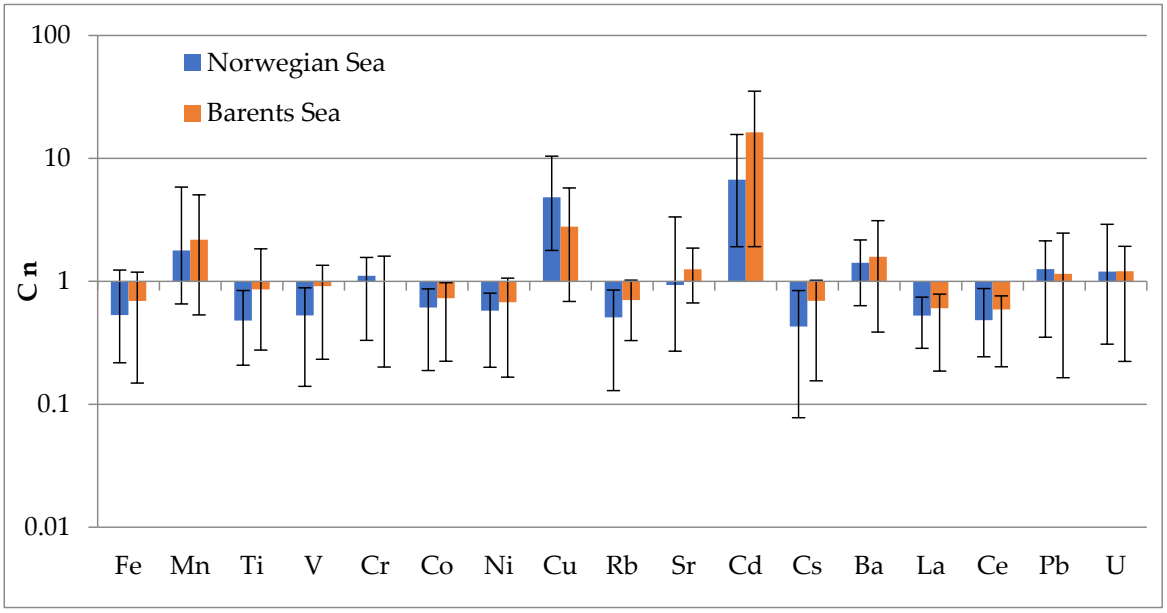

Figure 9. Average content of elements in SPM of BBL normalized to the composition of FLSM (C_n) and the range of variability of minimum and maximum values of C_n.

5. Conclusions

This study elucidates the biotic and abiotic processes affecting the cycling of trace elements in the Barents Sea and adjacent waters of the Norwegian Sea. The distribution and elemental composition of SPM in the euphotic layer of the Barents Sea are characterized by a significant mosaic pattern. The thickness of the euphotic layer varies by a factor of 4 within the shelf and depends on cloud cover and coccolithophorid blooming in the southern part of the sea. The distribution of calcifying phytoplankton in the water column of the Barents Sea is related to the increasing influence of the Atlantic water in the last two decades. Changes in the carbonate biological pump and Sr biogeochemical cycle are obvious in the vast southern part of the sea up to the Polar Front. Different groups of elements were distinguished, such as lithogenic (Fe, V, Ti, etc.), biogenic (Cd, U, and Sr), and hybrid (Mn, Cu, and Ba) elements. The lithogenic elements show a gradual increase in content in SPM with increasing depths. Bioessential elements reach their peak content in the SPM of the euphotic and subsurface water layer confined to the area of the thermocline. Hybrid distribution elements show a complex distribution pattern reaching maximum levels in the intermediate water layers influenced by both biogeochemical and physicochemical processes. In the Norwegian Sea, there is evidence to suggest an additional (hydrothermal) source for Mn, Ba, Cd, Cu, and Pb. Elements such as Mn, Cu, Sr, Cd, and Ba significantly enrich the particulate matter of the benthic nepheloid layer relative to the fluffy layer, which results from a substantial transformation of the suspended particle composition at the final stage of sedimentation. Ongoing climate change and Atlantification have implications for

the cycles of a number of trace elements, primarily Mn, Cu, Sr, Cd, Ba, etc., that have not yet been quantified.

Supplementary Materials: The following supporting information can be downloaded at: https://www.mdpi.com/article/10.3390/jmse11010065/s1, Table S1: SPM concentration, CTD data, and ICP-MS data on elemental composition of SPM; Table S2: Major phase composition of SPM; Table S3: Elemental composition of fluffy layer suspended matter.

Author Contributions: Conceptualization, M.D.K. and D.P.S.; methodology, D.P.S. and M.D.K.; validation, M.D.K. and S.V.V.; formal analysis, D.P.S.; investigation, A.I.K., A.S.L., N.M.M. and S.V.V.; resources, M.D.K.; data curation, A.I.K.; writing—original draft preparation, D.P.S., M.D.K. and S.V.V.; writing—review and editing, D.P.S. and M.D.K.; visualization, A.S.L.; supervision, M.D.K.; project administration, D.P.S.; funding acquisition, M.D.K. All authors have read and agreed to the published version of the manuscript.

Funding: The study and article preparation was supported through the grant of the Ministry of Science and Higher Education of the Russian Federation (grant no. 075-15-2021-934) "Study of anthropogenic and natural factors of changes in the composition of air and environmental objects in Siberia and the Russian sector of the Arctic in conditions of rapid climate change using unique scientific facility Tu-134 Optik Flying Laboratory". Field studies were carried out within the state assignment of the Shirshov Institute of Oceanology RAS (subject no. FMWE-2021-0006). The elemental analysis of particulate matter was supported by the Russian Science Foundation (project no. 20-17-00157).

Data Availability Statement: Not applicable.

Acknowledgments: The authors thank the crew of the RV Akademik Mstislav Keldysh, A.N. Novigatsky, S.V. Gladyshev, D.I. Frey, E.O. Zolotyh, G.V. Malafeev, and S.M. Isachenko for their help with water and sediment sampling, and O.N. Lukianova for help in the preparation of figures.

Conflicts of Interest: The authors declare no conflict of interest.

References

1. Lisitzin, A.P. *Oceanic Sedimentation: Lithology and Geochemistry*; American Geophysical Union Press: Washington, DC, USA, 1996; pp. 1–400. [CrossRef]
2. Jeandel, C.; van der Loeff, M.R.; Lam, P.J.; Roy-Barman, M.; Sherrell, R.M.; Kretschmer, S.; German, C.; Dehairs, F. What did we learn about ocean particle dynamics in the GEOSECS–JGOFS era? *Prog. Oceanogr.* **2015**, *133*, 6–16. [CrossRef]
3. Lam, P.J.; Lee, J.-M.; Heller, M.I.; Mehic, S.; Xiang, Y.; Bates, N.R. Size-fractionated distributions of suspended particle concentration and major phase composition from the U.S. GEOTRACES Eastern Pacific Zonal Transect (GP16). *Mar. Chem.* **2018**, *201*, 90–107. [CrossRef]
4. Hill, P.S.; Nowell, A.R.M. Comparison of two models of aggregation in continental-shelf bottom boundary layers. *J. Geophys. Res.* **1995**, *100*, 22749–22763. [CrossRef]
5. Etiope, G.; Favali, P.; Fuda, J.L.; Italiano, F.; Laubenstein, M.; Millot, C.; Plastino, W. The Benthic Boundary Layer: Geochemical and oceanographic data from the GEOSTAR-2 observatory. *Ann. Geophys.* **2006**, *49*, 705–713. [CrossRef]
6. Pempkowiak, J.; Bełdowski, J.; Pazdro, K.; Staniszewski, A.; Leipe, T.; Emeis, K.C. The contribution of the fine sediment fraction to the Fluffy Layer Suspended Matter (FLSM). *Oceanologia* **2002**, *44*, 513–527.
7. Ziervogel, K.; Forster, S. Aggregation and sinking behaviour of resuspended fluffy layer material. *Cont. Shelf Res.* **2005**, *25*, 1853–1863. [CrossRef]
8. Lein, A.Y.; Kravchishina, M.; Politova, N.; Savvichev, A.S.; Veslopolova, E.F.; Mitskevich, I.N.; Ul'Yanova, N.V.; Shevchenko, V.; Ivanov, M.V. Transformation of particulate organic matter at the water-bottom boundary in the Russian Arctic seas: Evidence from isotope and radioisotope data. *Lithol. Miner. Resour.* **2012**, *47*, 99–128. [CrossRef]
9. Pavlov, A.K.; Stedmon, C.A.; Semushin, A.V.; Martma, T.; Ivanov, B.V.; Kowalczuk, P.; Granskog, M.A. Linkages between the circulation and distribution of dissolved organic matter in the White Sea, Arctic Ocean. *Cont. Shelf Res.* **2016**, *119*, 1–13. [CrossRef]
10. Tsubouchi, T.; Våge, K.; Hansen, B.; Larsen, K.M.H.; Østerhus, S.; Johnson, C.; Jónsson, S.; Valdimarsson, H. Increased ocean heat transport into the Nordic Seas and Arctic Ocean over the period 1993–2016. *Nat. Clim. Chang* **2021**, *11*, 21–26. [CrossRef]
11. Overland, J.; Dunlea, E.; Box, J.E.; Corell, R.; Forsius, M.; Kattsov, V.; Olsen, M.S.; Pawlak, J.; Reiersen, L.-O.; Wang, M. The urgency of Arctic change. *Polar Sci.* **2019**, *21*, 6–13. [CrossRef]
12. Honeyman, B.D.; Balistrieri, L.S.; Murray, J. Oceanic trace metal scavenging: The importance of particle concentration. *Deep. Sea Res. Part A Oceanogr. Res. Pap.* **1988**, *35*, 227–246. [CrossRef]
13. Horner, T.J.; Little, S.H.; Conway, T.M.; Farmer, J.R.; Hertzberg, J.E.; Janssen, D.J.; Lough, A.J.M.; McKay, J.L.; Tessin, A.; Galer, S.J.G.; et al. Bioactive Trace Metals and Their Isotopes as Paleoproductivity Proxies: An Assessment Using GEOTRACES-Era Data. *Glob. Biogeochem. Cycles* **2021**, *35*, e2020GB006814. [CrossRef]

14. Pedersen, R.B.; Rapp, H.T.; Thorseth, I.H.; Lilley, M.D.; Barriga, F.; Baumberger, T.; Flesland, K.; Fonseca, R.; Früh-Green, G.L.; Jørgensen, S.L. Discovery of a black smoker vent field and vent fauna at the Arctic Mid-Ocean Ridge. *Nat. Commun.* **2010**, *1*, 126. [CrossRef]
15. Pedersen, P.B.; Bjerkgard, T. Massive sulphides in Arctic waters. In *Mineral Resources in the Arctic*; Boyd, R., Ed.; NGU Geological Survey of Norway: Trondheim, Norway, 2016; pp. 210–215.
16. Klyuvitkin, A.A.; Kravchishina, M.D.; Boev, A.G. Particle Fluxes in Hydrothermal Vent Fields of the Southern Part of the Mohns Ridge. *Dokl. Earth Sci.* **2021**, *497*, 200–205. [CrossRef]
17. Shevchenko, V.P.; Lein, A.Y.; Zernova, W.; Ivanov, G.I.; Lisitzin, A.P. The distribution and composition of suspended matter and phytoplankton in the surface layer of Norwegian and Greenland seas in august 1996. *Dokl. Earth Sci.* **1997**, *335*, 805–807.
18. Shevchenko, V.P.; Burovkin, A.A.; Zernova, V.V.; Shanin, S.S.; Ivanov, G.I.; Polyak, L.V.; Dzhinoridze, R.N. Sedimentary material flows in the St. Anna Trough and Eastern Barents Sea. *Dokl. Earth Sci.* **1998**, *359A*, 400–403.
19. Aibulatov, N.A.; Matyushenko, V.A.; Shevchenko, V.P.; Politova, N.V. New data on the transverse structure of lateral flows of the suspended material along the Barents Sea periphery. *Environ. Geosci.* **1999**, *6*, 526–540. (In Russian)
20. Lukashin, V.N.; Bogdanov, Y.A.; Shevchenko, V.P.; Rusakov, V.Y.; Isaeva, A.B. A study of vertical fluxes of sedimentary material and its composition in the Norwegian Sea in the summer periods of 1991–1995. *Geochem. Int.* **2000**, *38*, 169–183.
21. Lukashin, V.N. Geochemistry of suspended matter and sinking material in the eastern Norwegian Sea. *Geochem. Int.* **2008**, *46*, 711–723. [CrossRef]
22. Lukashin, V.N. Sedimentary matter fluxes in the contour current sedimentation system over the continental slope of the Norwegian Sea. *Oceanology* **2008**, *48*, 701–709. [CrossRef]
23. Politova, N.V.; Shevchenko, V.P.; Zernova, V.V. Distribution, Composition, and Vertical Fluxes of Particulate Matter in Bays of Novaya Zemlya Archipelago, Vaigach Island at the End of Summer. *Adv. Meteorol.* **2012**, *2012*, 259316. [CrossRef]
24. Murdmaa, I.O.; Bogdanova, O.Y.; Gorshkov, A.I.; Novikov, G.V.; Shevchenko, V.P. Iron and Manganese Minerals in Suspended Matter from the Barents Sea. *Lithol. Miner. Resour.* **2000**, *35*, 594–597. [CrossRef]
25. Politova, N.V.; Kravchishina, M.D.; Novigatsky, A.N.; Lokhov, A.S. Dispersed Sedimentary Matter of the Barents Sea. *Oceanology* **2019**, *59*, 697–714. [CrossRef]
26. Shevchenko, V.P.; Politova, N.V.; Aibulatov, N.A. Quantitative distribution and compistion of suspended matter in the coastal area of the Pechora Sea. In *The Mankind and the Coastal Zone of the World Ocean in XXI Century*; Aibulatov, N.A., Ed.; GEOS: Moscow, Russia, 2000; pp. 23–250. (In Russian)
27. Shevchenko, V.P.; Politova, N.V.; Aibulatov, N.A. Water suspended matter and its fluxes. In *The Pechora Sea: Systematic Research (Hydrophysics, Hydrology, Optics, Bilogy, Chemistry, Geology, Ecology, Social and Economic Issues)*; Romankevich, E.A., Ed.; More: Moscow, Russia, 2003; pp. 247–262. (In Russian)
28. Politova, N.V. Features of the Distribution and Composition of Suspended Particulate Matter and Sedimentary Fluxes in the Barents and Pechora Seas. Ph.D. Thesis, Shirshov Institute of Oceanology RAS, Moscow, Russia, 30 October 2007. (In Russian).
29. Pfirman, S.L. Modern Sedimentation in the Northern Barents Sea: Input, Dispersal, and Deposition of Suspended Sediments from Glacial Meltwater. Ph.D. Thesis, Massachusetts Institute of Technology, The Woods Hole Oceanographic Institution, Woods Hole, MA, USA, August 1984. [CrossRef]
30. Buettner, S.; Ivanov, V.V.; Kassens, H.; Kusse-Tiuz, N.A. Distribution of suspended particulate matter in the Barents Sea in late winter 2019. *Arct. Antarct. Res.* **2020**, *66*, 267–278. [CrossRef]
31. Rusakov, V.Y.; Lisitsyn, A.P.; Izotova, S.S.; Moskalev, A.S.; Gazenko, A.O.; Rahold, F. Distribution and mineral composition of particulate matter in the Franz Victoria Trough (Northern Barents Sea). *Oceanology* **2004**, *44*, 247–256.
32. Matishov, G.G.; Mityaev, M.V.; Khasankaev, V.B.; Tarasov, G.A.; Golubev, V.A. Regions of recent sedimentary material accumulation in the Medvezhii Trench, Barents Sea. *Dokl. Earth Sci.* **2002**, *385*, 567–569.
33. Lukashin, V.N.; Shcherbinin, A.D. Hydrological properties, suspended matter, and particulate fluxes in the water column of the Bear Island Trough. *Oceanology* **2007**, *47*, 68–79. [CrossRef]
34. Ivanov, G.I. *Geoecology of Western Arctic Shelf of Russia: Lithological and Ecogeochemical Aspects*; Nauka: Saint-Petersburg, Russia, 2006; pp. 1–303. (In Russian)
35. McPhee, E.E.; Nowell, A.R.; Sternberg, R.W. Boundary layer measurements and their implications for sediment transport on the eastern Norwegian Sea continental slope. *Deep Sea Res.* **1998**, *45*, 719–743. [CrossRef]
36. Frey, D.I.; Novigatsky, A.N.; Kravchishina, M.D.; Morozov, E.G. Water structure and currents in the Bear Island trough in July–August 2017. *Russ. J. Earth Sci.* **2017**, *17*, ES3003. [CrossRef]
37. King, E.L.; Bøe, R.; Bellec, V.K.; Rise, L.; Skarðhamar, J.; Ferré, B.; Dolan, M.F. Contour current driven continental slope-situated sandwaves with effects from secondary current processes on the Barents Sea margin offshore Norway. *Mar. Geol.* **2014**, *353*, 108–127. [CrossRef]
38. Loeng, H. Features of the physical oceanographic conditions of the Barents Sea. *Polar Res.* **1991**, *10*, 5–18. [CrossRef]
39. Pisarev, S.V. Review of the Barents Sea hydrological conditions. In *Barents Sea System*; Lisitzin, A.P., Ed.; GEOS: Moscow, Russia, 2021; pp. 153–166. (In Russian) [CrossRef]
40. Lind, S.; Ingvaldsen, R.B.; Furevik, T. Arctic warming hotspot in the northern Barents Sea linked to declining sea-ice import. *Nat. Clim. Chang* **2018**, *8*, 634–639. [CrossRef]

41. Polyakov, I.V.; Rippeth, T.P.; Fer, I.; Alkire, M.B.; Baumann, T.M.; Carmack, E.C.; Ingvaldsen, R.; Ivanov, V.V.; Janout, M.; Lind, S.; et al. Weakening of Cold Halocline Layer Exposes Sea Ice to Oceanic Heat in the Eastern Arctic Ocean. *J. Clim.* **2020**, *33*, 8107–8123. [CrossRef]
42. Kopelevich, O.V.; Sahling, I.V.; Vazyulya, S.V.; Glukhovets, D.I.; Sheberstov, S.V.; Burenkov, V.I.; Karalli, P.G.; Yushmanova, A.V. *Bio-Optical Characteristics of the Seas, Surrounding the Western Part of Russia, from Data of the Satellite Ocean Color Scanners of 1998–2017*; OOO "VASh FORMAT": Moscow, Russia, 2018; pp. 1–42. (In Russian)
43. Kopelevich, O.; Sheberstov, S.; Vazyulya, S. Effect of a Coccolithophore Bloom on the Underwater Light Field and the Albedo of the Water Column. *J. Mar. Sci. Eng.* **2020**, *8*, 456. [CrossRef]
44. Kopelevich, O.V.; Vazyulya, S.V.; Gluhovets, D.I.; Saling, I.V. Biooptical characteristics and solar radiation in the surface layer of the Barents Sea. In *Barents Sea System*; Lisitzin, A.P., Ed.; GEOS: Moscow, Russia, 2021; pp. 236–245. (In Russian) [CrossRef]
45. Pautova, L.A.; Silkin, V.A.; Kravchishina, M.D.; Chultsova, A.L.; Lisitzin, A.P. The Biological Calcium Carbonate Pump in the Norwegian and Barents Seas: Regulation Mechanisms. *Dokl. Earth Sci.* **2020**, *490*, 46–50. [CrossRef]
46. Silkin, V.; Pautova, L.; Giordano, M.; Kravchishina, M.; Artemiev, V. Interannual variability of Emiliania huxleyi blooms in the Barents Sea: In situ data 2014–2018. *Mar. Pollut. Bull.* **2020**, *158*, 111392. [CrossRef]
47. Review Ice Charts for the Arctic Ocean. Available online: http://old.aari.ru/odata/_d0015.php?lang=1&mod=0&yy=2017 (accessed on 9 December 2022).
48. Jakobsson, M.; Mayer, L.A.; Bringensparr, C.; Castro, C.F.; Mohammad, R.; Johnson, P.; Ketter, T.; Accettella, D.; Amblas, D.; An, L.; et al. The International Bathymetric Chart of the Arctic Ocean Version 4.0. *Sci. Data* **2020**, *7*, 176. [CrossRef]
49. Kravchishina, M.D.; Novigatskii, A.N.; Savvichev, A.S.; Pautova, L.A.; Lisitsyn, A.P. Studies on Sedimentary Systems in the Barents Sea and Norwegian–Greenland Basin during Cruise 68 of the R/V Akademik Mstislav Keldysh. *Oceanology* **2019**, *59*, 158–160. [CrossRef]
50. Schlitzer, R. *Ocean Data View*; AWI: Bremerhaven, Germany, 2021.
51. Krishnaswami, S.; Sarin, M. Atlantic surface particulates: Composition, settling rates and dissolution in the deep sea. *Earth Planet. Sci. Lett.* **1976**, *32*, 430–440. [CrossRef]
52. Gelman, E.M.; Starobina, I.Z. *Photometric Methods for Determining Rock-Forming Elements in Ores, Rocks and Minerals*; GEOKHI AS USSR: Moscow, Russia, 1976; pp. 1–69. (In Russian)
53. Rudnick, R.L.; Gao, S. Composition of the Continental Crust. In *Treatise on Geochemistry*; Rudnick, R.L., Holland, H.D., Turekian, K.K., Eds.; Elsevier: Amsterdam, The Netherlands, 2003; Volume 3, pp. 1–64.
54. Lukashin, V.N.; Krechik, V.A.; Klyuvitkin, A.A.; Starodymova, D.P. Geochemistry of Suspended Particulate Matter in the Marginal Filter of the Pregolya River (Baltic Sea). *Oceanology* **2018**, *58*, 856–869. [CrossRef]
55. Kopelevich, O.V.; Vazyulya, S.V.; Grigoriev, A.V.; Khrapko, A.N.; Sheberstov, S.V.; Sahling, I.V. Penetration of visible solar radiation in waters of the Barents Sea depending on cloudiness and coccolithophore blooms. *Oceanology* **2017**, *57*, 402–409. [CrossRef]
56. Hancke, K.; Hovland, E.K.; Volent, Z.; Pettersen, R.; Johnsen, G.; Moline, M.; Sakshaug, E. Optical properties of CDOM across the Polar Front in the Barents Sea: Origin, distribution and significance. *J. Mar. Syst.* **2014**, *130*, 219–227. [CrossRef]
57. Glukhovets, D.; Kopelevich, O.; Yushmanova, A.; Vazyulya, S.; Sheberstov, S.; Karalli, P.; Sahling, I. Evaluation of the CDOM Absorption Coefficient in the Arctic Seas Based on Sentinel-3 OLCI Data. *Remote Sens.* **2020**, *12*, 3210. [CrossRef]
58. Smyth, T.J.; Tyrrell, T.; Tarrant, B. Time series of coccolithophore activity in the Barents Sea, from twenty years of satellite imagery. *Geophys. Res. Lett.* **2004**, *31*, L11302. [CrossRef]
59. Pautova, L.A.; Silkin, V.A.; Kravchishina, M.D.; Yakubenko, V.G.; Chultsova, A.L. Summer phytoplankton of the northern Barents Sea (75–80° N). *Hydrosphere Ecol.* **2019**, *2*, 8–19. (In Russian) [CrossRef]
60. Kravchishina, M.D.; Novigatsky, A.N.; Savvichev, A.S.; Pautov, L.A.; Lisitzin, A.P. Sedimentation systems definition of the Barents Sea and Norwegian-Greenland basin during 68th cruise of the research vessel Academic Mstislav Keldysh. *Okeanologiya* **2019**, *59*, 173–176. [CrossRef]
61. Box, J.E.; Colgan, W.T.; Wouters, B.; Burgess, D.O.; O'Neel, S.; Thomson, L.I.; Mernild, S.H. Global sea-level contribution from Arctic land ice: 1971–2017. *Environ. Res. Lett.* **2018**, *13*, 125012. [CrossRef]
62. Faust, J.C.; Stevenson, M.A.; Abbott, G.D.; Knies, J.; Tessin, A.; Mannion, I.; Ford, A.; Hilton, R.; Peakall, J.; März, C. Does Arctic warming reduce preservation of organic matter in Barents Sea sediments? *Philos. Trans. R. Soc.* **2020**, *378*, 20190364. [CrossRef] [PubMed]
63. Lisitsin, A.P.; Shevchenko, V.P.; Burenkov, V.I. Hydrooptics and suspended matter of Arctic seas. *Atmos. Ocean. Opt.* **2000**, *13*, 61–71.
64. Kravchishina, M.D.; Lein, A.Y.; Sukhanova, I.N.; Artem'Ev, V.A.; Novigatsky, A.N. Genesis and spatial distribution of suspended particulate matter concentrations in the Kara Sea during maximum reduction of the Arctic ice sheet. *Oceanology* **2015**, *55*, 623–643. [CrossRef]
65. Laukert, G.; Makhotin, M.; Petrova, M.V.; Frank, M.; Hathorne, E.C.; Bauch, D.; Böning, P.; Kassens, H. Water mass transformation in the Barents Sea inferred from radiogenic neodymium isotopes, rare earth elements and stable oxygen isotopes. *Chem. Geol.* **2019**, *511*, 416–430. [CrossRef]
66. Bogdanov, Y.A.; Sagalevitch, A.M.; Galkin, S.M.; Tchernyaev, E.S.; Lukashin, V.N.; Ivanov, G.V. Geological and biological investigation in the northern part of the Mohn's Ridge (Norwegian Sea). *Oceanology* **1997**, *37*, 548–555.

67. Lobus, N.V.; Kulikovskiy, M.S.; Maltsev, Y.I. Multi-Element Composition of Diatom *Chaetoceros* spp. from Natural Phytoplankton Assemblages of the Russian Arctic Seas. *Biology* **2021**, *10*, 1009. [CrossRef] [PubMed]
68. Duhamel, S.; Diaz, J.M.; Adams, J.C.; Djaoudi, K.; Steck, V.; Waggoner, E.M. Phosphorus as an integral component of global marine biogeochemistry. *Nat. Geosci.* **2021**, *14*, 359–368. [CrossRef]
69. Mart, L.; Nürnberg, H.W.; Rützel, H. Comparative Studies on Cadmium Levels in the North Sea, Norwegian Sea, Barents Sea and the Eastern Arctic Ocean. In *Environmental Research and Protection*; Fresenius, W., Lüderwald, I., Eds.; Springer: Berlin/Heidelberg, Germany, 1984; pp. 201–209. [CrossRef]
70. Bruland, K.W.; Lohan, M.C. Controls of trace metals in seawater. In *Treatise on Geochemistry: The Oceans and Marine Geochemistry*; Elderfield, H., Ed.; Elsevier: New York, NY, USA, 2004; Volume 6, pp. 23–47.
71. Ho, T.-Y.; Quigg, A.; Finkel, Z.V.; Milligan, A.J.; Wyman, K.; Falkowski, P.G.; Morel, F.M.M. The elemental composition of some marine phytoplankton1. *J. Phycol.* **2003**, *39*, 1145–1159. [CrossRef]
72. Simpson, W. A critical review of Cadmium in the Marine environment. *Prog. Oceanogr.* **1981**, *10*, 1–70. [CrossRef]
73. Zheng, Y.; Anderson, R.F.; van Geen, A.; Fleisher, M.Q. Preservation of particulate non-lithogenic uranium in marine sediments. *Geochim. Cosmochim. Acta* **2002**, *66*, 3085–3092. [CrossRef]
74. Zheng, Y.; Anderson, R.F.; van Geen, A.; Fleisher, M.Q. Remobilization of authigenic uranium in marine sediments by bioturbation. *Geochim. Cosmochim. Acta* **2002**, *66*, 1759–1772. [CrossRef]
75. Stoll, H. Calcification rate and temperature effects on Sr partitioning in coccoliths of multiple species of coccolithophorids in culture. *Glob. Planet. Chang* **2002**, *34*, 153–171. [CrossRef]
76. Paasche, E. A review of the coccolithophorid Emiliania huxleyi (Prymnesiophyceae), with particular reference to growth, coccolith formation, and calcification-photosynthesis interactions. *Phycologia* **2001**, *40*, 503–529. [CrossRef]
77. Tebo, B.M.; Bargar, J.R.; Clement, B.G.; Dick, G.J.; Murray, K.J.; Parker, D.; Verity, R.; Webb, S.M. BIOGENIC MANGANESE OXIDES: Properties and Mechanisms of Formation. *Annu. Rev. Earth Planet. Sci.* **2004**, *32*, 287–328. [CrossRef]
78. Ingri, J. Geochemistry of ferromanganese concretions in the Barents Sea. *Mar. Geol.* **1985**, *67*, 101–119. [CrossRef]
79. Dehairs, F.; Chesselet, R.; Jedwab, J. Discrete suspended particles of barite and the barium cycle in the open ocean. *Earth Planet. Sci. Lett.* **1980**, *49*, 528–550. [CrossRef]
80. Bishop, J.K.B. The barite-opal-organic carbon association in oceanic particulate matter. *Nature* **1988**, *332*, 341–343. [CrossRef]
81. Jeandel, C.; Tachikawa, K.; Bory, A.; Dehairs, F. Biogenic barium in suspended and trapped material as a tracer of export production in the tropical NE Atlantic (EUMELI sites). *Mar. Chem.* **2000**, *71*, 125–142. [CrossRef]
82. Steinsund, P.I.; Hald, M. Recent calcium carbonate dissolution in the Barents Sea: Paleoceanographic applications. *Mar. Geol.* **1994**, *117*, 303–316. [CrossRef]
83. Emelyanov, E.M. *Barrier Zones in the Ocean*; Springer: Berlin/Heidelberg, Germany; New York, NY, USA, 2005; pp. 1–636.